BRAIN
A JOURNAL OF NEUROLOGY

Microglial activation correlates *in vivo* with both tau and amyloid in Alzheimer's disease

Melanie Dani,[1] Melanie Wood,[1] Ruth Mizoguchi,[1] Zhen Fan,[1] Zuzana Walker,[2,3] Richard Morgan,[4] Rainer Hinz,[5] Maya Biju,[6] Tarun Kuruvilla,[6] David J. Brooks[1,7,8] and Paul Edison[1]

Alzheimer's disease is characterized by the histopathological presence of amyloid-β plaques and tau-containing neurofibrillary tangles. Microglial activation is also a recognized pathological component. The relationship between microglial activation and protein aggregation is still debated. We investigated the relationship between amyloid plaques, tau tangles and activated microglia using PET imaging. Fifty-one subjects (19 healthy controls, 16 mild cognitive impairment and 16 Alzheimer's disease subjects) participated in the study. All subjects had neuropsychometric testing, MRI, amyloid (^{18}F-flutemetamol), and microglial (^{11}C-PBR28) PET. All subjects with mild cognitive impairment and Alzheimer's disease and eight of the controls had tau (^{18}F-AV1451) PET. ^{11}C-PBR28 PET was analysed using Logan graphical analysis with an arterial plasma input function, while ^{18}F-flutemetamol and ^{18}F-AV1451 PET were analysed as target:cerebellar ratios to create parametric standardized uptake value ratio maps. Biological parametric mapping in the Statistical Parametric Mapping platform was used to examine correlations between uptake of tracers at a voxel-level. There were significant widespread clusters of positive correlation between levels of microglial activation and tau aggregation in both the mild cognitive impairment (amyloid-positive and amyloid-negative) and Alzheimer's disease subjects. The correlations were stronger in Alzheimer's disease than in mild cognitive impairment, suggesting that these pathologies increase together as disease progresses. Levels of microglial activation and amyloid deposition were also correlated, although in a different spatial distribution; correlations were stronger in mild cognitive impairment than Alzheimer's subjects, in line with a plateauing of amyloid load with disease progression. Clusters of positive correlations between microglial activation and protein aggregation often targeted similar areas of association cortex, indicating that all three processes are present in specific vulnerable brain areas. For the first time using PET imaging, we show that microglial activation can correlate with both tau aggregation and amyloid deposition. This confirms the complex relationship between these processes. These results suggest that preventative treatment for Alzheimer's disease should target all three processes.

1   Neurology Imaging Unit, Department of Medicine, Imperial College London, Hammersmith Hospital, UK
2   Division of Psychiatry, University College London, UK
3   Essex Partnership University NHS Foundation Trust, UK
4   Chelsea and Westminster Hospital, London, UK
5   Wolfson Molecular Imaging Centre, University of Manchester, UK
6   ²Gether NHS Foundation Trust, Gloucester, UK
7   Department of Nuclear Medicine, Aarhus University, Denmark
8   Institute of Neuroscience, University of Newcastle upon Tyne, UK

Correspondence to: Dr Paul Edison MD, MRCP, PhD, FRCP, FRCPI
Neurology Imaging Unit
Division of Brain Sciences
Imperial College London

DuCane Road, Hammersmith Hospital, London, W12 0NN
UK
E-mail: paul.edison@imperial.ac.uk

Introduction

Despite extensive research in recent decades, no cure has been identified for Alzheimer's disease, and the precise mechanisms of the underlying pathologies are still unclear. Cardinal pathological features are amyloid-β plaques and neurofibrillary tangles composed of hyperphosphorylated tau (Perl, 2010; Serrano-Pozo *et al.*, 2011*a*). A third feature, which is also important in the disease process, is microglial activation. Microglial cells are the intrinsic macrophages of the CNS and are responsible for monitoring and responding to injury and insult in the surrounding brain (Pasqualetti *et al.*, 2015). Activated microglial cells surround abnormally aggregated protein and are thought to represent the brain's natural defence mechanism as they attempt to clear the protein fibrils. In Alzheimer's disease and other neurodegenerative diseases, microglial activation becomes persistent and eventually ineffective (Heneka *et al.*, 2015; Pasqualetti *et al.*, 2015). In addition, the products of microglia chronically activated by aggregated amyloid-β (pro-inflammatory cytokines such as tumour necrosis factor α, interleukin-6, interleukin-1α, granulocyte macrophage-colony stimulating factor) can cause toxic damage to surrounding cells, the severity of which increases as disease progresses (Serrano-Pozo *et al.*, 2016). Histopathological studies have shown that activated microglial cells surround amyloid plaques (Perlmutter *et al.*, 1990; Stalder *et al.*, 1999) and neurofibrillary tangles (Sheffield *et al.*, 2000; Serrano-Pozo *et al.*, 2011*b*), possibly in an attempt to clear them. However, other studies suggest that microglial activation may be an early process in disease pathogenesis, causing abnormal protein aggregation (Yoshiyama *et al.*, 2007; Lee *et al.*, 2015). The precise role of microglial activation and in particular its relationship to amyloid deposition and tau aggregation is still debated.

Given that amyloid deposition plateaus around the time of onset of symptoms (Villemagne *et al.*, 2013) and that in established disease persistent microglial activation may lead to neuronal damage and tau aggregation (Sheffield *et al.*, 2000), we hypothesized that levels of microglial activation would correlate with neurofibrillary tangle load in established Alzheimer's disease, while in mild cognitive impairment (MCI), microglial activation would correlate with amyloid deposition.

PET imaging allows us to detect and quantify microglial activation, amyloid deposition and tau aggregation *in vivo*, and provides spatial information about the extent of these molecular processes—information that was only previously available at end-stage post-mortem. Additionally, advanced image processing and quantification using Biological Parametric Mapping (Casanova *et al.*, 2007) allows us to interrogate the inter-relationship between these processes at a voxel level. ^{18}F-flutemetamol PET is a marker of fibrillar amyloid-β (Ikonomovic *et al.*, 2016) while ^{18}F-AV1451 PET is a high affinity marker of paired helical filament-tau (Xia *et al.*, 2013). ^{11}C-PBR28 PET is a marker of translocator protein (TSPO), which is expressed by the outer mitochondrial membrane of the activated microglia associated with Alzheimer's disease (Kreisl *et al.*, 2013*a*).

The aim of this study was to evaluate *in vivo* the spatial inter-relationship between microglial activation, tau aggregation, and amyloid deposition in MCI and Alzheimer's disease subjects.

Materials and methods

Study population

This study was approved by national and local ethics committees: the Riverside Research Ethics Committee, National Health Research Services, Health Research Authority, UK. Approval for administration of PET tracers was obtained from the Administration of Radioactive Substances Advisory Committee (ARSAC). Written informed consent was obtained from all subjects.

Recruitment

Subjects were recruited from local memory clinics, a national dementia recruitment website and advertisements in local media. After providing informed consent, subjects underwent a screening visit, and their clinical diagnosis of MCI and Alzheimer's disease was confirmed after checking the clinical and neurological findings, MRI scans and neuropsychometric evaluation. The Petersen criteria (Petersen *et al.*, 2004) were used for the diagnosis of MCI subjects, while NIA-AA (National Institute of Ageing and Alzheimer's Association; McKhann *et al.*, 2011) or NINCDS-ADRDA (National Institute of Neurological and Communicative Disorders and Stroke-AD and Related Disorders Association criteria; McKhann *et al.*, 1984) were used for the diagnosis of Alzheimer's disease. Subjects were then stratified according to whether they carried one or two copies of the Ala147Thr polymorphism of the *TSPO* gene as high affinity binders, mixed

affinity binders, or low affinity binders of ^{11}C-PBR28 (Owen *et al.*, 2012). Low affinity binders were excluded from the study.

Inclusion criteria were: (i) a diagnosis of MCI according to the Petersen criteria, or Alzheimer's disease fulfilling NINCDS-ADRDA or NIA-AA criteria, or normal cognition for the healthy controls; (ii) age range 50–85 years; (iii) ability to give informed consent; (iv) at least 8 years of formal education; and (v) Mini-Mental State Examination score >24 for MCI, >15 for Alzheimer's disease, and normal cognition for healthy controls. Exclusion criteria were: (i) history of major depression, or any significant disease influencing neuropsychological testing; (ii) schizophrenia or schizoaffective disorder; (iii) inability to undergo MRI scanning, and (iv) a malignancy within the last 5 years (except localized skin or prostate cancer).

Fifty-one subjects (19 healthy controls, 16 MCI and 16 clinical Alzheimer's disease subjects) participated in the study. Along with neuropsychometric testing and MRI scanning, all subjects had ^{18}F-flutemetamol PET, and 18 of 19 had ^{11}C-PBR28 PET. All MCI and Alzheimer's disease subjects and seven of the controls had ^{18}F-AV1451 PET.

Image acquisition

MRI

Subjects had MRI with a 3 T Siemens Verio scanner and a 32-channel head coil. A T_1-weighted magnetization prepared rapid gradient echo sequence (MPRAGE) (repetition time = 2400 ms, echo time = 3.06 ms, flip angle of 9, inversion time = 900 ms, matrix = 256×246) with a 1 mm^3 voxel size, anteroposterior phase encoding direction, and a symmetric echo was used. Two subjects with coronary artery stents (who were therefore ineligible for 3 T MRI) underwent 1.5 T MRI with a Philips Achieva system at the MRC Clinical Sciences Centre, Imperial College London.

PET imaging

[11]C-PBR28

[11]C-PBR28 was manufactured at the Imanova Centre for Imaging Sciences in London and imaging was performed at the same centre with a Siemens Truepoint PET/CT (axial field of view of 21.8 cm; 111 transaxial planes; spatial resolution of 2.056 mm $\times$ 2.056 mm $\times$ 2 mm after image reconstruction). A mean dose of 330.9 ($\pm$ 30) MBq of ^{11}C-PBR28 in 20 ml normal saline was injected. Dynamic data were acquired in 3D and list mode over 90 min and the data were rebinned using the following time frames; 8×15 s, 3×60 s, 5×120 s, 5×300 s, 5×600 s. Arterial blood was sampled (via a radial artery cannula) continuously with an online detector for the first 15 min and discrete blood samples were taken at 5, 10, 20, 30, 50, 70 and 90 min. Samples were centrifuged to measure whole blood and plasma radioactivity along with radioactive metabolite levels. Reverse-phase chromatography was used to analyse plasma metabolites. Data reconstruction was performed by filtered back projection, (2.6 zoom, and 5 mm Gaussian filter).

[18]F-flutemetamol

[18]F-flutemetamol was made by GE Healthcare. Scans were performed at Imperial College Clinical Imaging Facility using a Siemens Biograph 6 scanner with a 15-cm field of view. A mean dose of 183.4 ($\pm$5.3) MBq of ^{18}F-flutemetamol was injected in 8 ml saline followed by a 10 ml saline flush. Data were acquired in 3D list mode from 90 to 120 min following injection (6×5 min frames). Image reconstruction was performed by filtered back projection with attenuation correction. Post reconstruction 5 mm Gaussian smoothing was performed. The zoom was 2.6, the matrix size was 168×168 and the pixel size was 1.56 mm $\times$ 1.56 mm $\times$ 1.92 mm.

^{18}F-AV1451

^{18}F-AV1451 was manufactured at Imanova Centre for Imaging Sciences, London, and scans were acquired using the same Siemens Truepoint PET/CT scanner as for ^{11}C-PBR28 PET. A mean dose of 168.3 ($\pm$7.4) MBq ^{18}F-AV1451 was injected in 20 ml saline. Data were acquired in 3D list mode for 120 min (frames of 8×15 s, 3×60 s, 5×120 s, 5×300 s, 8×600 s). Data reconstruction was performed with iterative reconstruction and 5 mm Gaussian smoothing was applied post reconstruction.

Image processing

MRI and PET scans were preprocessed using Analyze AVW 11.0. Image processing was performed in Analyze AVW 11.0 and Statistical Parametric Mapping 5 (SPM5, Wellcome Trust Centre for Neuroimaging, University College London) on a MATLAB platform. Voxel level correlations were interrogated using the Biological Parametric Mapping toolbox, which is integrated into SPM software. ^{11}C-PBR28 parametric V_T images were created with in-house MICK.exe parametric mapping software 'MICK' (Modelling, Input functions and Compartmental Kinetics) version 5.2 software [available on request from Wolfson Molecular Imaging Centre, University of Manchester, Manchester, UK (Dr Rainer Hinz)] was used to fit all regional compartmental models with the Nelder-Mead optimization algorithm (Nelder and Mead, 1965). MICK uses MATLAB R2009bSP1 (The MathWorks, Natick, MA, USA) (Fan *et al.*, 2016; McGinnity *et al.*, 2017).

[11]C-PBR28 processing

Logan graphical analysis was used to create parametric maps of V_T at a voxel level using metabolite corrected arterial plasma input functions and dynamic PET time–activity curves for each subject. MICK software was used to generate a parametric map of ^{11}C-PBR28 V_T from the slope of the Logan plot (Logan, 2000). The V_T map was then co-registered to the T_1-weighted volumetric MRI scan, and transformed into Montreal Neurologic Institute standard space.

[18]F-flutemetamol and ^{18}F-AV1451

The 90–120 min summed ^{18}F-flutemetamol and 80–100 min summed ^{18}F-AV1451 PET images were co-registered to their T_1-weighted MRI, and transformed into Montreal Neurological Institute space. The individual's MRI was

segmented into grey matter, white matter and CSF using Analyze AVW. Grey matter voxels were defined as having >50% probability of being grey matter and Analyze AVW was used to create individualized grey matter binary images. The binarized image was then convolved with the Hammers probabilistic atlas (Hammers *et al.*, 2003) to create an individualized object map. The cerebellum was then sampled, and target-to-cerebellar uptake ratio images were produced by dividing the summed image by the uptake of cerebellar grey matter uptake in Analyze AVW. Region of interest analysis was performed by sampling these ratio images using individualized object maps.

PET images were analysed both with and without a partial volume correction for reduction due to any atrophy present in the MRIs of MCI and Alzheimer disease subjects. Partial volume correction was performed by structural-functional synergy for resolution recovery (SFS-RR) on a MATLAB platform (Shidahara *et al.*, 2009).

Voxel-level group comparisons

Normalized co-registered PET images (target:cerebellar ratio images for ^{18}F-AV1451 and ^{18}F-flutemetamol and Logan V_T parametric maps for ^{11}C-PBR28) for each disease group were compared to the controls using an independent *t*-test in SPM. A *P*-value of <0.05 was considered significant, and no voxel extent threshold was used. For ^{11}C-PBR28 PET, each group was compared to the respective control group according to binding status.

Additionally, to identify whether each individual was 'positive' for tracer binding, a single-subject comparison was performed in SPM as an independent *t*-test compared to the mean of the respective control group.

Determining amyloid status

Based on region of interest analysis of their SUVR ^{18}F-flutemetamol images, subjects were classified as amyloid-positive or negative. Subjects were classified as amyloid-positive if they had increased binding [compared to control mean + 2 standard deviations (SD)] in one or more cortical regions (frontal, parietal, temporal, occipital lobe, anterior cingulate and posterior cingulate cortex). This was confirmed on visual read. Subjects were deemed positive for tau tangles and microglial activation if they had increased tracer binding (relative to control mean + 2 SD) in the left or right hippocampus, parahippocampus, amygdala, fusiform gyrus, temporal lobe, frontal lobe, parietal lobe, or occipital lobe.

Generation of Z-score maps and voxel-level correlations using biological parametric mapping analysis

The biological parametric mapping toolbox (Casanova *et al.*, 2007) was used to create Z-score maps of tracer uptake for each subject. Generating tracer Z-maps for each subject allows spatial correlations between the uptake of the different tracers with different means and variances to be interrogated and reveals the inter-relationships of each Alzheimer pathology.

The Z-score maps were created in SPM5 using the following formulae:

$$\text{Z-score } (^{11}\text{C-PBR28 } V_T) = (^{11}\text{C-PBR28 Logan } V_T \text{ of individual-mean of the control } ^{11}\text{C-PBR28 Logan } V_T)/ \quad (1)$$
$$\text{SD of}^{11}\text{C-PBR28 control Logan } V_T$$

$$\text{Z-score } (^{18}\text{F-flutemetamol}) = \text{individual } ^{18}\text{F-flutemetamol ratio image-control mean of } ^{18}\text{F-} \quad (2)$$
$$\text{flutemetamol ratio / SD of control } ^{18}\text{F-flutemetamol}$$

$$\text{Z-score } (^{18}\text{F-AV1451}) = \text{individual}^{18}\text{F-AV1451 ratio-} \quad$$
$$\text{control mean of } ^{18}\text{F-} \quad (3)$$
$$\text{AV1451 ratio/SD of control } ^{18}\text{F-AV1451}$$

For ^{11}C-PBR28 images, Z-maps were generated from the appropriate control cohort according to the TSPO binding status of each subject. ^{11}C-PBR28 uptake of MCI and Alzheimer's disease cases who were high or mixed affinity binders was compared with mean uptake of the high or mixed affinity binders in the control group. After Z-maps were generated (so accounting for effects of binding status), the medium and high affinity binders were then combined for analysis as one group.

The voxel-level correlations between microglial activation, amyloid load, and tau aggregation were interrogated across individual Z-score maps using the Biological Parametric Mapping toolbox for all groups. To assess significance of correlations between ^{18}F-flutemetamol and ^{11}C-PBR28 uptake, and ^{18}F-AV1451 and ^{11}C-PBR28 uptake in the amyloid-negative subjects, a statistical threshold was set at $P < 0.05$ with an extent threshold of 500 voxels. Given the highly significant positive correlations between ^{18}F-AV1451 and ^{11}C-PBR28 in the amyloid-positive MCI and Alzheimer's disease groups, we set the cluster level of significance at 0.01, and the extent threshold at 500 voxels for these correlation analyses. All clusters with a corrected *P*-value of $P < 0.05$ were considered significant. *P*-values were corrected for family-wise errors.

Data availability

The authors confirm that the data supporting the findings of this study are available within the article and its Supplementary material.

Results

Demographics

All 19 healthy controls in our 51 subjects scanned were amyloid-negative. Nine MCI subjects were amyloid-positive while seven were negative. Of the 16 subjects with a clinical diagnosis of Alzheimer's disease, 14 were amyloid-positive and two were negative. These two subjects had a clinical diagnosis of probable Alzheimer's disease based on the NINCDS-ADRDA criteria, but had negative amyloid PET

scans. Both individuals had impaired neuropsychometric tests in multiple domains that affected activities of daily life. The MRIs of both subjects showed reduced hippocampal volume. Their diagnoses were made in a hospital clinic setting, and were reconfirmed on the initial screening visit.

Table 1 shows the demographic and neuropsychometric details of the cohort. As expected, neuropsychometric tests revealed impaired scores for both MCI and Alzheimer's disease subjects. The mean delay between ^{18}F-flutemetamol and ^{11}C-PBR scans was 2.1 months; and ^{18}F-AV1451 and ^{11}C-PBR28 scans was 8 months. The amyloid-positive MCI subjects were significantly older than the amyloid-negative subjects, with significantly worse delayed visual recall, delayed word list recall and semantic fluency.

Voxel-level group differences

Figure 1 shows the voxel-level distribution of increased ^{18}F-flutemetamol, ^{18}F-AV1451 and ^{11}C-PBR28 uptake (only the high affinity binders are shown for ^{11}C-PBR28 as these represented the majority of these cases—eight of the Alzheimer's disease cases, four of the MCI cases and seven of the amyloid-negative cases compared to the control group).

Although the clusters show trends for increased uptake, there were no significantly increased clusters in the Alzheimer's disease or amyloid-negative group compared to the controls at a group level.

However, when we examined tracer uptake for each individual compared to the control group, distinct binding patterns emerged. In the Alzheimer's disease group (all of whom were amyloid-positive), five had increased tau and microglial activation; nine only had increased tau. In the amyloid-positive MCI group, four had increased tau, while two had increased microglial activation and one had both increased tau and microglial activation. In the amyloid-negative group, three individuals had increased tau and microglial activation, two had increased microglial activation

and one had increased tau only. Clusters of each individual's increase binding for ^{11}C-PBR and ^{18}F-AV1451 are shown in Supplementary Table 4. There were six individuals (five Alzheimer's disease and one amyloid-positive MCI) who had increased binding of all three tracers.

To visually display the spatial distributions of tracer binding, the mean summed images are shown for each group and each tracer in Supplementary Fig. 1. Data for the 18 healthy control subjects who had ^{11}C-PBR28 PET (11 high affinity binders and seven mixed affinity binders) are shown in Supplementary Fig. 4.

Voxel-level correlations

There were clusters of highly significant positive correlations throughout the cortex between microglial activation and both tau aggregation and amyloid deposition in the Alzheimer's disease and MCI subjects (Figs 2 and 3). There were extensive clusters of positive correlations, with a larger area of involvement and higher Z-scores, between microglial activation and tau aggregation compared with microglial activation and amyloid deposition. There were also clusters of positive correlations between microglial activation and tau aggregation in the amyloid-negative group throughout the isocortex. (Fig. 2)

Tau and microglial activation

Amyloid-positive individuals

Positive correlations between ^{18}F-AV1451 and ^{11}C-PBR28 uptake are shown in Supplementary Table 1. In the MCI group, there were positive correlations in the frontal, temporal, parietal and cingulate but not the occipital cortices. The strongest correlations in the group, with the highest Z-scores and correlation coefficients, were in the frontal lobe.

In the Alzheimer's disease group, there were significant positive correlations between ^{18}F-AV1451 and ^{11}C-PBR28

Table 1 Demographics of the study cohort

	Controls (n = 19)	Amyloid-positive MCI (n = 9)	Amyloid-negative MCI (n = 7)	Alzheimer's disease (n = 16)
Age	64.22 (8.52)	76.62 (5.07)**	68.71 (7.48)	73.69 (7.15)*
Years education	13.37 (3.34)	14.14 (3.98)	11.25 (0.96)	12.92 (2.74)
Mini-Mental State Examination (total = 30)	29.41 (1.06)	28.33 (1.22)	26.71 (2.06)*	21.62 (3.28)**
Delayed visual recall (total = 36)	18.18 (7.12)	10.44 (6.32)*	19.29 (3.67)	5.19 (6.33)**
Delayed word list recall (total = 12)	10.21 (2.04)	2.22 (1.99)**	6.86 (3.34)*	1.14 (1.70)**
Word list recognition (total = 12)	11.27 (1.03)	7.67 (3.57)	8.29 (3.63)	3.64 (3.13)
Semantic fluency	20.73 (6.00)	13.33 (4.03)*	19.29 (5.82)	10.93 (6.13)**
Trail-making A	35.24 (10.83)	51.22 (11.71)	52.43 (25.44)*	107.67 (120)
Trail-making B	74.13 (23.0)	171.67 (106)**	116.33 (39.80)**	148 (46)*
Right hippocampal volume, mm^3	3860 (407)	3398 (574)	3669 (477)	2827 (549)**
Left hippocampal volume, mm^3	3745 (333)	3199 (779)*	3662 (267)	2743 (400)**
White matter hypointensity volume, mm^3	2160 (1208)	3693.5 (1771)	9898 (18658)	5153 (3296)**

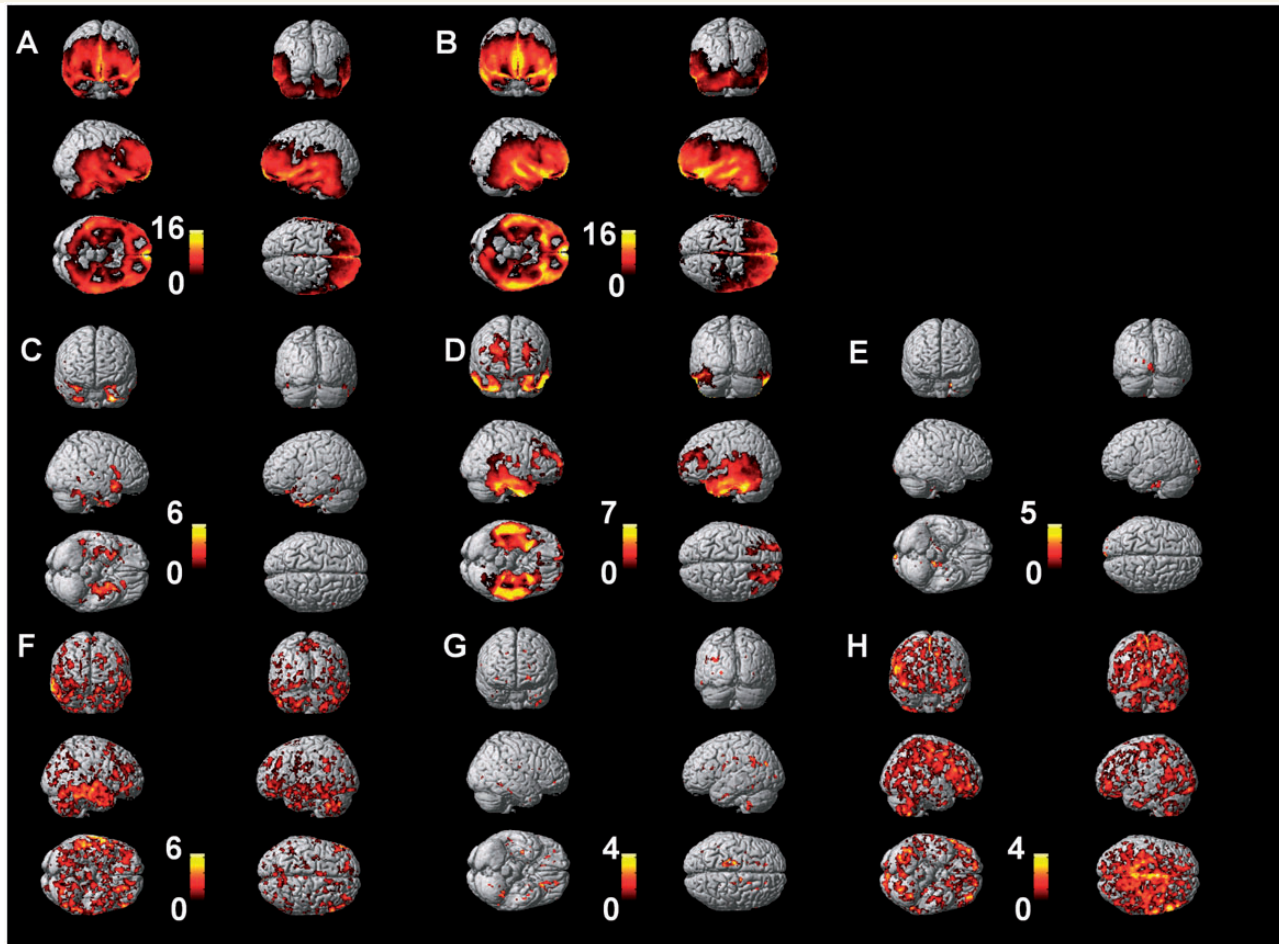*$P < 0.05$; **$P < 0.01$. Values represent mean (SD).

Figure 1 Distributions of amyloid, tau and microglial activation. This figure shows voxel level increases in each tracer compared to the controls. **A** and **B** show voxel level increases in ^{18}F-flutemetamol in MCI and Alzheimer's disease, respectively. **C–E** show increases in ^{18}F-AV1451 in amyloid-positive MCI, Alzheimer's disease and amyloid-negative individuals. **F–H** show increased ^{11}C-PBR28 in high affinity binders compared to controls in amyloid-positive individuals, Alzheimer's disease and amyloid-negative individuals, respectively. For ^{18}F-flutemetamol and ^{11}C-PBR28, a threshold of significance of $P < 0.05$ was used. For ^{18}F-AV1451, a threshold of significance of $P < 0.01$ was used.
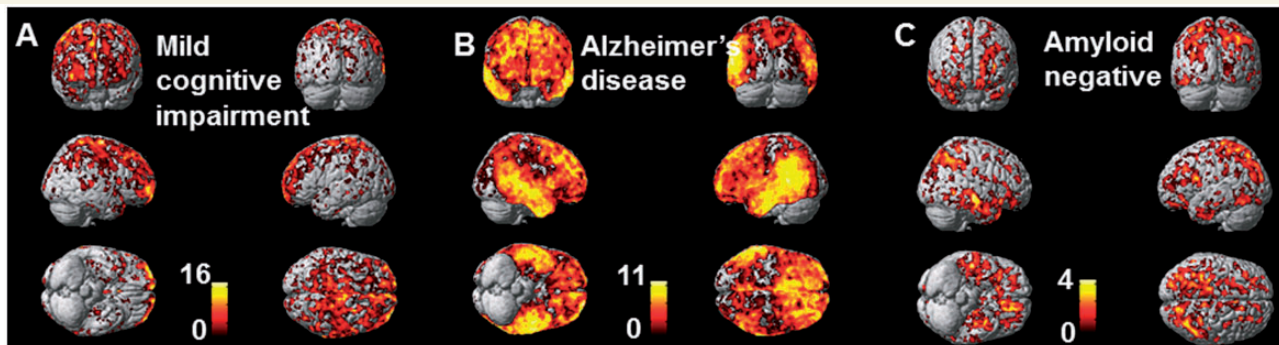

Figure 2 Correlations between tau and microglial activation. Voxel level correlations between tau and microglial activation in the amyloid-positive MCI (**A**), Alzheimer's disease (**B**) and amyloid-negative cognitively-impaired individuals (**C**).

uptake in the frontal, temporal, parietal, occipital, and insular cortices. The strongest correlations were seen in the frontal and temporal lobes and the Z-scores were higher in the Alzheimer's disease compared to the MCI group,

indicating increasing tau-inflammation correlations at voxel level as the disease advances.

The clusters of positive correlations in the temporal lobe differed between the MCI and Alzheimer's disease groups:
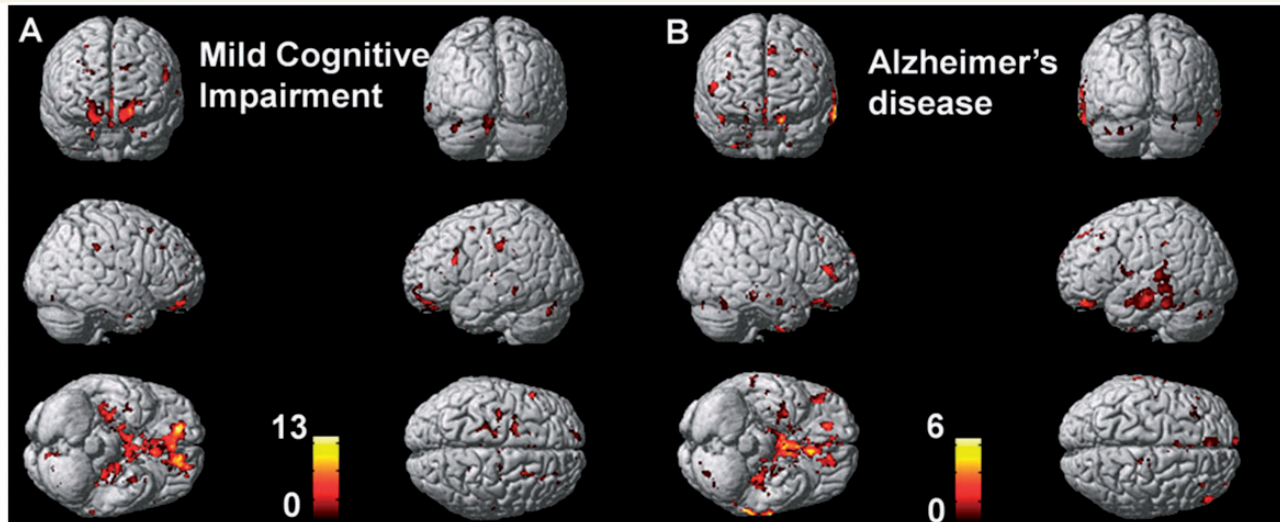
Figure 3 Correlations between amyloid deposition and microglial activation. Voxel level correlations between amyloid and microglial activation in the amyloid-positive MCI (**A**) and Alzheimer's disease (**B**) individuals.

the MCI group had positive clusters in the posterior temporal lobes and left fusiform gyrus while the distribution was more diffuse in the Alzheimer's disease group—the anterior, posterior, lateral (fusiform gyrus) and medial temporal (amygdala and hippocampus) lobes all had clusters of significant correlation (Supplementary Table 1).

Examples of correlation plots from individual single voxels within clusters are shown in Supplementary Fig. 3. Correlation plots from the voxels with the highest Z-scores and correlation coefficients have been illustrated.

Amyloid-negative individuals

There were two individuals with a clinical diagnosis of Alzheimer's disease who were amyloid-negative. The results for these subjects were combined with the amyloid-negative MCI individuals when performing the Biological Parametric Mapping correlation analysis, as they were likely to represent non-Alzheimer syndromes. Individual voxel level increases of tau aggregation and microglial activation for the nine individuals are shown in Fig. 5. Positive correlations are shown in Supplementary Table 1.

Tau aggregation and microglial activation were positively correlated in this group, with clusters in the right superior parietal gyrus, left posterior temporal lobe, left lateral part of occipital lobe and right superior frontal gyrus. The areas of positive correlation were smaller with lower Z-scores and lower correlation coefficients than those seen for the amyloid-positive groups.

Amyloid and microglial activation

Amyloid-positive individuals

There were positive correlations throughout the cortex in both Alzheimer's disease and MCI subjects. However, MCI subjects showed more extensive regions of correlation with higher correlation coefficients and Z-scores compared to

the Alzheimer's disease group. The most widespread distribution of positive correlations in the MCI group was in the frontal and temporal cortex, while in the Alzheimer's disease group, the parietal cortex had the widest distribution of clusters. The locations of regions of positive correlations are shown in Supplementary Table 1 and Fig. 3.

Regions where microglial activation correlated with both tau aggregation and amyloid deposition

Certain regions had clusters of positive correlations between microglial activation and both amyloid deposition and tau aggregation across all the groups (MCI and Alzheimer's disease, amyloid-positive and negative). These regions included the posterior temporal lobe and superior frontal gyrus. Other regions that were commonly affected in more than one group were the lateral part of the occipital lobe and inferolateral part of the parietal lobe.

Tracer-positive individuals only

Next, to ensure that our correlations were not false positives arising from inclusion of 'null data points' from tracer negative individuals, and to address the fact that there were not significant differences between the Alzheimer's disease group and controls, we analysed the six individuals (one MCI and five Alzheimer's disease individuals) who were positive at voxel level for binding of all three tracers. As the number of these subjects was small, they were analysed as a single group. Correlations and group differences with controls for each tracer are shown in Supplementary Table 2. Individual levels of microglial activation correlated strongly with levels of both amyloid deposition and tau aggregation across the cortex, with Z-scores above 4 (Fig. 4). The clusters with
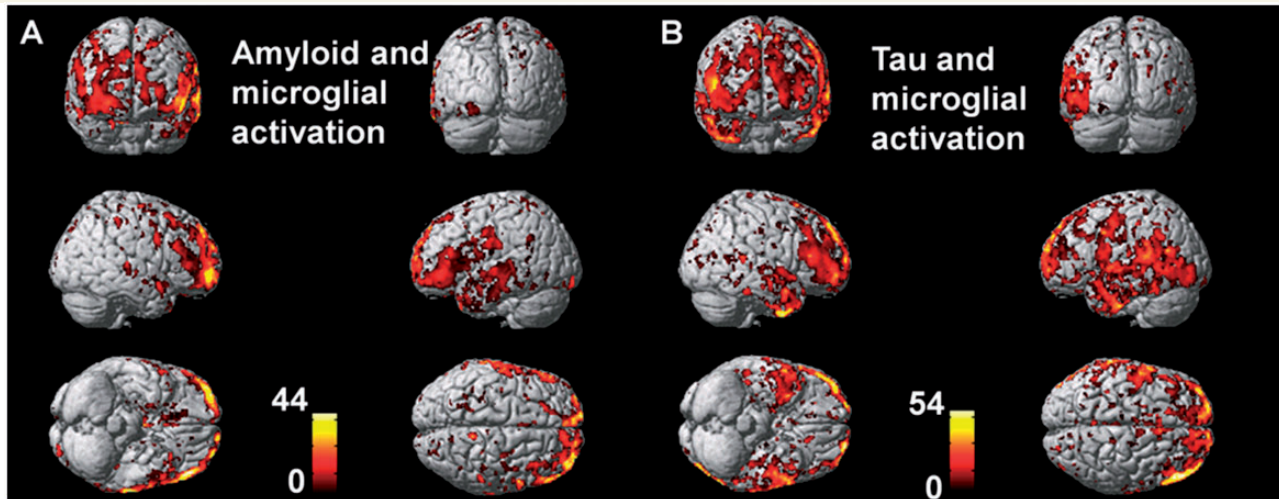
Figure 4 Correlations in the tracer-positive individuals only. The figure shows voxel-level correlations in the individuals who were positive for all three tracers. **A** shows correlations between microglial activation and tau aggregation, and **B** shows correlations between microglial activation and amyloid deposition.
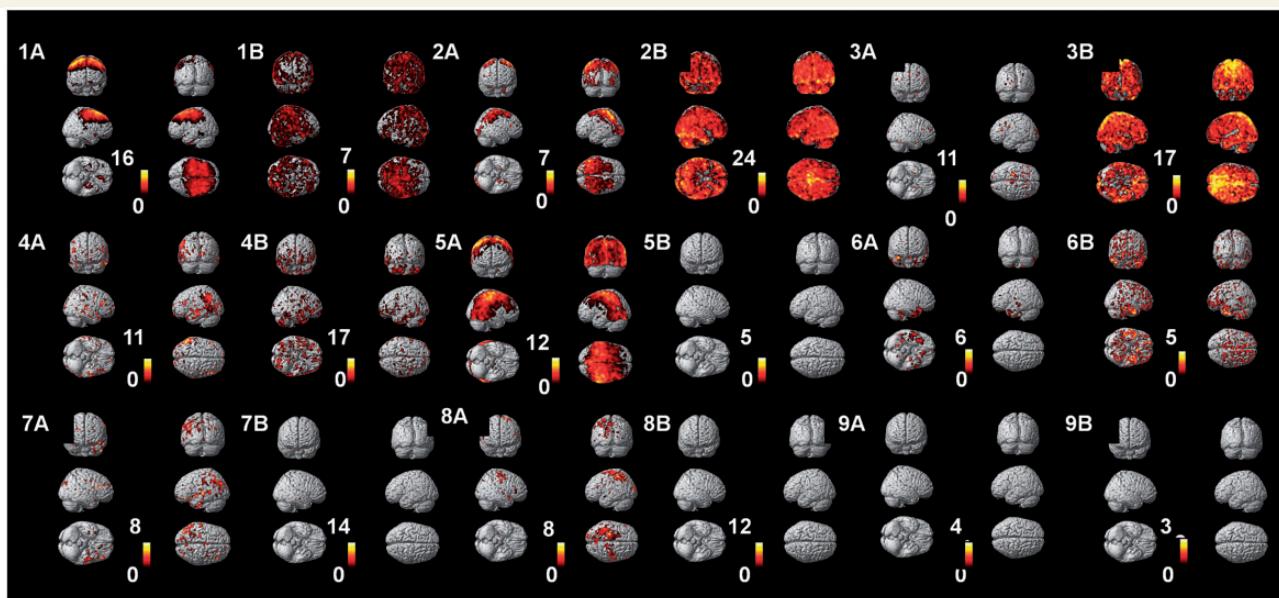

Figure 5 Distributions of microglial activation and tau aggregation in the amyloid-negative individuals. Individual parametric maps (Individuals 1–9) of microglial activation (**A**) and tau aggregation (**B**) in the nine amyloid-negative individuals with cognitive impairment, compared to the control mean. Clusters show trends of increased binding. Individuals 1, 2, and 4–6 had statistically significant clusters of ^{18}F-AV1451 binding, while Individuals 1–4 and 6 had statistically significant ^{11}C-PBR28 binding compared to the control groups. This figure is provided to illustrate distributions of the pathologies in this small group of individuals.

the strongest correlations between amyloid and microglial activation were localized in the precentral, inferior and middle frontal gyri. The strongest correlations between tau and microglial activation were localized in the superior, middle and inferior frontal gyri.

The clusters of positive correlations between tau and microglial activation were of a similar size, correlation strength and distribution in this small subgroup.

Partial volume correction of images

Clusters of correlated uptake across the tracers using partial volume corrected images are shown in Supplementary Table 3 and Fig. 2. Interestingly, when partial volume correction was applied, the correlations became more widespread and showed higher Z-scores and r-correlation coefficients than the non-partial volume corrected images.

The pattern of positive correlations, and the stronger correlation between microglial activation and tau aggregation in Alzheimer's disease than MCI persisted.

Discussion

In this first reported PET study to examine microglial activation, tau aggregation and amyloid deposition in subjects with MCI and Alzheimer's disease, we found clusters where microglial activation is strongly correlated at a voxel level with both tau aggregation and amyloid deposition. There were also significant positive correlations between tau aggregation and microglial activation in our amyloid-negative cognitively impaired group.

Correlations between tau aggregation and microglial activation were stronger in the Alzheimer's disease group compared to the MCI group, with higher Z-scores, higher correlation coefficients (r) and a wider distribution of clusters, particularly in the temporal lobe where tau aggregation is known to increase in intensity through the Braak stages (Braak and Braak, 1991). These findings support previous histopathological and in vitro studies, which have shown that microglial activation parallels tau aggregation as disease progresses (Sheffield et al., 2000; Serrano-Pozo et al., 2011b). In addition, microglial activation correlates with the spread of tau aggregation in the brain (Maphis et al., 2015b). The pro-inflammatory products of microglial activation promote tau hyperphosphorylation in vitro (Quintanilla et al., 2004; Gorlovoy et al., 2009; Lee et al., 2010; Maphis et al., 2015b), which in turn induces tau neurofibrillary tangle formation; this may then cause further microglial activation (Zilka et al., 2009) resulting in a positive feedback cycle as disease progresses (Fig. 6). This could apply to our MCI/Alzheimer's disease cohort, however, longitudinal studies are needed to provide more insight into mechanisms driving progression of disease rather than a cross-sectional study.

Clusters of correlations between amyloid and microglial activation were predominantly localized in the isocortex i.e. the frontal, temporal, parietal and occipital, insular and anterior cingulate cortices. These findings support previous histopathological findings that have described microglia surrounding cortical amyloid plaques (Perlmutter et al., 1990; Stalder et al., 1999). Interestingly, the area of distribution was wider and the strength of correlations was higher in the MCI subjects compared to the Alzheimer's disease group. This may be because amyloid deposition occurs early in the disease process triggering microglial activation in an attempt to clear the plaques. A peak of early microglial activation could occur when amyloid deposition first takes place a decade before symptoms appear (Villemagne et al., 2013) followed by a decline in microglial activation as amyloid load plateaus, followed by a second peak as neurofibrillary tangles form and intensify across the cortex (Serrano-Pozo et al., 2011b).

The fact that tau aggregation and microglial activation were correlated in our amyloid-negative individuals (albeit less strongly than in the amyloid-positive individuals) suggests that amyloid is not necessary for a cycle of tau tangle–activated microglia–tau tangle feedback. Microglial activation may drive tauopathies playing a similar underlying pathogenic role to that in Alzheimer's disease i.e. promoting tau hyperphosphorylation and propagation in the brain. This is in line with previous in vivo findings of increased microglial activation in tauopathies (Paulus et al., 1993; Ishizawa and Dickson, 2001; Ishizawa et al., 2004). The consistent pattern of inflammation seen in cognitively impaired tau-positive individuals who were positive and negative for amyloid, suggests that the findings are not due to false positives.

Two amyloid-negative dementia subjects had a clinical diagnosis of Alzheimer's disease based on NINCDS-ADRDA criteria, and cognitive impairment in multiple domains, affecting activities of daily life. Both had evidence of elevated ^{18}F-AV1451 binding in the temporal lobe substructures (on sampling of the ratio image), and both had elevated ^{11}C-PBR28 V_T calculated from a two-tissue compartment model (data not shown). While these individuals are unlikely to have Alzheimer's disease (according to their biomarker profile), they represent a significant proportion of Alzheimer's disease 'mimics'. Clinical trials and autopsy studies show that 15–16% of individuals with a diagnosis of 'probable Alzheimer's disease' have insufficient neuropathological changes to confirm the diagnosis (Salloway et al., 2014; Serrano-Pozo et al., 2014). Notably, when examining the distributions of tau aggregation and microglial activation in each of the nine individuals, the distributions and patterns of each tracer differed, emphasizing the heterogeneity of pathologies in these individuals. This group was small, with only three individuals demonstrating increased binding of both ^{11}C-PBR28 and ^{18}F-AV1451, and there were no group mean differences from the controls in either pathology. However, five individual subjects had increased microglial activation and four had increased tau aggregation compared with the controls, emphasizing the heterogeneity of pathologies in these individuals. One possible diagnosis could be primary age-related tauopathy (PART) where isolated neurofibrillary tangles are localized to the medial temporal lobe, across a spectrum of cognitive ability (Crary et al., 2014), although microglial activation has not been reported in this condition. Microglial activation can play a role in other neurodegenerative diseases such as dementia with Lewy bodies, frontotemporal dementia and Parkinson's disease (Cagnin et al., 2004; Surendranathan et al., 2015). Additionally, mixed pathologies in the ageing brain are very common (Schneider et al., 2009) and the relationship between microglial activation and other senile pathologies such as TDP-43 aggregation, hippocampal sclerosis and argyrophilic grain disease are still unknown. Finally, small vessel disease can be associated with microglial activation, which is a well-recognized

subacute response to stroke (Vidale *et al.*, 2017; Zhao *et al.*, 2017) and occurs after cerebral hypoperfusion in mice (Manso *et al.*, 2018). Thus, the presence of microglial activation in both patients with and without amyloid may be related to independent processes altogether, with tau hyperphosphorylation representing the end of a final common pathway.

Although this study was not longitudinal, so inferences about temporal changes in the disease process cannot be made, it is interesting that amyloid load correlated with inflammation levels most strongly in MCI whereas tau load correlated most strongly with inflammation levels in Alzheimer's disease by which time amyloid plaque load has plateaued but tau tangles are still increasing. *In vitro* studies suggest that microglial activation may actually cause upregulation of both tau and amyloid pathology (Lee *et al.*, 2015), again supporting the positive feedback mechanism, and explaining the rapid progression of cortical neurofibrillary tangles in Alzheimer's disease. Furthermore, tau protein in a pathological form may actually be required for microglia-induced cell toxicity, showing again the complex interplay between the pathologies (Maphis *et al.*, 2015a). While the clusters of positive correlations are indicative of the relative timing of pathologies i.e. that peaks of microglial activation occur as first amyloid and then tau aggregation increases in the cortex, the exact temporal and spatial patterns of disease cannot be inferred from this cross-sectional data and a longitudinal follow-up study is required.

While our data shed some light on the relative distributions and correlations of microglial activation in MCI and Alzheimer's disease, the relationship between amyloid plaques, tau tangles and microglial activation is clearly complex. Recent reports suggest that cortical amyloid plaque deposition is required to promote isocortical, though not subcortical, tau aggregation in a synergistic manner so driving disease progression (Pascoal *et al.*, 2017). Recent biomarker studies (Pontecorvo *et al.*, 2017) and older histopathological work (Price and Morris, 1999) show that amyloid deposition and tau aggregation start independently of each other (amyloid in the isocortical areas, tau neurofibrillary tangles in the medial temporal lobe), but that the spread of tau to the isocortical areas is dependent on the presence of amyloid fibrils. The spatial dissociation of this synergism is unexplained, but may be due to amyloid cross-seeding tau along functional networks and precipitating tau spread (Vasconcelos *et al.*, 2016). The role of microglial activation is likely to be critical in this process e.g. microglial cells activated by amyloid plaques may induce further tau hyperphosphorylation, inducing further neurofibrillary tangles and initiating tau spread across the cortex, leading to Alzheimer's disease (represented in Fig. 6). It is important to note that not all areas follow this model, and imaging data may not fully reflect the spectrum of heterogeneity of pathology in Alzheimer's disease. Hopefully, autoradiographic and histopathological follow-up of our imaging dataset will provide support for this hypothesis.

Microglial activation may at times play a protective role: a mouse study crossing transgenic amyloid and transgenic tau mice produced offspring with increased microglial
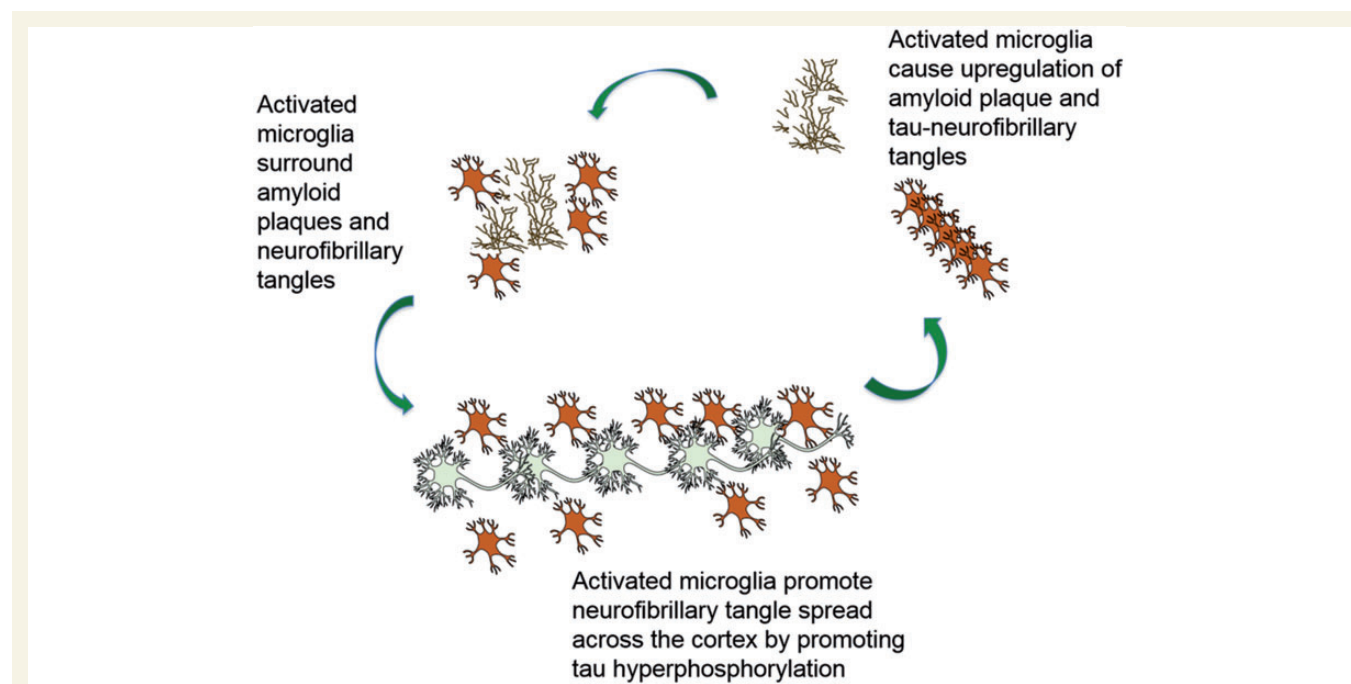

Figure 6 The vicious cycle of activated microglia and protein aggregation. Activated microglia surround amyloid plaque and neurofibrillary tangles, and in turn promote upregulation of amyloid plaque and tangles. Further, the pro-inflammatory products of activated microglia promote further tau hyperphosphorylation and spreading of neurofibrillary tangles throughout the cortex.

activation (and increased phagocytic ability), and a 40–50% reduced plaque load, implying that under certain circumstances tau-induced microglia activation clears amyloid load (Chen et al., 2016). However, current PET tracers are unable to differentiate between protective or detrimental roles of activated microglia.

The use of ^{11}C-PBR28 PET as a marker of TSPO expression and, indirectly, microglial activation should also be discussed. ^{11}C-PBR28 has a sub-nanomolar affinity for a binding site on TSPO expressed by the mitochondria of activated microglia which is 80 times higher than the affinity of the first generation ligand ^{11}C-PK11195 (Kreisl et al., 2010). It has differentiated Alzheimer's disease from healthy controls in several studies (Kreisl et al., 2013b; Lyoo et al., 2015) but no studies to date have shown increased uptake in MCI subjects. Binding has been shown to increase with Alzheimer disease progression (Kreisl et al., 2016), and has been shown to correlate with extent of neurodegeneration in the primary visual cortex of posterior cortical atrophy cases (Kreisl et al., 2017). However, there are also limitations. No studies to date have shown group regional V_T differences between Alzheimer's disease, MCI and controls. High variability is also a feature of ^{11}C-PBR28 PET (Cumming et al., 2018). A study in healthy controls showed high test-retest variability ($15.9 \pm 12.2\%$), high intersubject variability and significant differences in results when scanning the same subjects in the morning and afternoon (Collste et al., 2016). However, another study examining ^{11}C-PBR28 in multiple sclerosis found a lower absolute mean test-retest variability ranging from 7% to 9% (Park et al., 2015). Other studies have shown that there are significant correlations between peripheral leucocyte count and brain TSPO binding, suggesting that TSPO expression may be susceptible to systemic immune changes (Kanegawa et al., 2016). The variable free fraction of tracer in the plasma may introduce another source of variance. This variability may be one reason for the lack of group differences between the Alzheimer's disease group and healthy controls in our cohort. Moreover, a blocking study showed tracer binding throughout the brain, indicates that there is no region in the brain that is truly devoid of binding that can be used as a reference for non-specific binding (Owen et al., 2014).

Furthermore, there is evidence that levels of microglial activation fluctuate with Alzheimer's disease progression (Fan et al., 2017). There is evidence of increased microglial activation early on (Hamelin et al., 2016), which plateaus (Lopez-Picon et al., 2018), followed by further activation later in the disease course (Fan et al., 2017). Our cohort was imaged at a single time point so it is not possible to ascertain the exact stage of disease trajectory that each individual is on, with a mean Mini-Mental State Examination score of 22, our Alzheimer's disease cohort had relatively mild or 'intermediate' disease, which may also explain the low levels of microglial activation in some individuals and the lack of group difference.

The TSPO receptor is used as a biomarker marker for neuroinflammation but, as well as being expressed by activated microglia, TSPO can also become upregulated in other cells including astroglia and neurons. It is possible that the correlations we see with PBR28 PET between intracellular tau tangle and activated microglia load reflect TSPO expression by dystrophic neurons; however, histopathological studies on Alzheimer brains would be against this. Rather, our results are in line with histopathological studies that show activated microglia surround neurofibrillary tangles (Sheffield et al., 2000; Serrano-Pozo et al., 2011b). Autoradiographic studies are required to confirm that our results do not represent false-positive co-localization. Finally, a recent study examining the effects of myeloid cell activation on TSPO expression found that activation of pro-inflammatory macrophages in humans is associated with a reduction in TSPO expression (in contrast to rodents, where the converse was seen) (Owen et al., 2017). This study indicates a possible limitation in using the TSPO receptor as a neuroinflammation marker.

Several different analytical methods have been used with ^{11}C-PBR28 PET. Studies have reported conflicting results, which is partly due to different methodological approaches. Groups have corrected V_T for the free fraction of ^{11}C-PBR28 in plasma and reported significant differences between patients and control subjects (Kreisl et al., 2013b). Other groups have used the cerebellum as a 'pseudo-reference region', arguing that Alzheimer pathology occurs late in the cerebellum so any pathological changes in early cases will be seen in the isocortex (Lyoo et al., 2015). Groups using ^{11}C-PBR28 PET to study other diseases have used 'whole brain binding' as a reference region (Bloomfield et al., 2016) in order to reduce variance due to genotypic and plasma protein binding variability. However, as there is no cortical region devoid of translocator protein, this approach will act to diminish observed relative changes in target regions. A whole brain reference region of interest will also reflect signal from white matter and subcortical structures (Narendran and Frankle, 2016).

Another factor to consider with ^{11}C-PBR28 is correction for free fraction of the tracer in plasma (fP, which may account for some of the variability introduced by plasma input function).

In our cohort, fP ranged from 0.78% to 2.89%, and there were no significant differences in fP between the three groups (mean value for free fraction of tracer in plasma = 1.829, SD = 0.478; coefficient of variation 26%). This high variability is similar to previous reports (Hines et al., 2013; Rizzo et al., 2014). Some authors argue that the very small values of fP can lead to inaccuracies in measurement and laboratory error (Rizzo et al., 2014; Turkheimer et al., 2015). The effect of fP levels only becomes critical, however, if exchange rates of ^{11}C-PBR28 on and off plasma proteins is of the same order or slower than its rate of brain uptake. Generally, exchange of tracers on and off plasma proteins is rapid compared to rates of their brain uptake and so has relatively little influence on brain

V_Ts. Having said that, a study using ^{11}C-PK11195 found that this isoquinoline tracer strongly bound to some plasma proteins, which are upregulated in inflammatory diseases (Lockhart et al., 2003). This may confound measurement of TSPO binding in inflammatory diseases such as Alzheimer's disease.

As such, and in view of the lack of consensus agreement about whether V_T or V_T/fP is superior (Cumming et al., 2018), we have reported V_T (rather than V_T/fP).

Thus, it is clear that there are limitations associated with the use of ^{11}C-PBR28 PET, and results should be interpreted with caution. In view of the fact that there is no true reference region in the brain for TSPO binding, we chose to compute absolute quantification using an arterial plasma input function as this remains the gold standard for PET analysis.

One of the strengths of our study is that our disease groups were clinically well characterized with detailed neuropsychometric evaluation and known amyloid status. In addition, we used an arterial input function to analyse ^{11}C-PBR28 V_T. We also accounted for the differential binding status of subjects for ^{11}C-PBR28 due to differential expression of TSPO polymorphisms (Owen et al., 2012; Kreisl et al., 2013a; Yoder et al., 2013) by creating z-maps for each individual's binding compared to the controls. This allowed all subjects to be examined as a group whether classified as mixed- or high-affinity binders. We excluded the low-affinity binders from the study (due to their negligible binding) but it has recently been demonstrated that binding status is not associated with clinical status, therefore conclusions from a subgroup can be applied to a whole cohort (Fan et al., 2015). However, the spectrum in binding affinity remains a limitation of the second generation TSPO tracers, and other unidentified genetic sources of variation may also be present.

One of the limitations of our study was that for the ^{11}C-PBR28 and ^{18}F-flutemetamol PET scans, the MCI and Alzheimer's disease groups were significantly older than our healthy control group. While some studies have suggested that microglial activation increases with age (Kumar et al., 2012; Walker et al., 2015), other PET studies have not detected a significant increase with age (Suridjan et al., 2014). Additionally, we did not find a correlation between microglial activation and age in our healthy control group. Second, because of patient and scanner availability and the onerous nature of the study, there were time delays between scans. During these months, the pathological processes may have progressed, but we assume this would not have been considerable given the long duration of these processes.

Individuals taking benzodiazepines were excluded from the study. One individual in the Alzheimer's disease group was taking a non-steroidal anti-inflammatory medication and it was not recorded whether a dose was taken on the day of the scan. This may represent a potential confound affecting ^{11}C-PBR binding, although this individual had significantly higher uptake than the mean +2 SD of the control group.

Additionally, while the correlations between tracer binding in this cohort are intriguing, we acknowledge the fact that there were no significant between-group mean differences between the Alzheimer's disease group and amyloid-negative group and healthy controls. This is a limitation of the study, and may be due to the high variability in ^{11}C-PBR28 described above, the dynamic nature of microglial activation or the fact that the study is small and underpowered to detect group level differences, particularly when subdividing groups according to amyloid status, disease group and binding status. However, our subgroup analysis of tracer-positive individuals confirmed that correlations across tracer uptake did not artefactually arise from 'null data points' from tracer-negative individuals.

We acknowledge that the numbers used in the study are too small to make a definitive conclusion about the distribution of these processes in Alzheimer's disease. This is particularly apparent when dividing groups according to disease status and amyloid status. If we had larger numbers of individuals with increased binding of all three tracers, a more robust correlative analysis could be performed. However, these findings are important and may guide future work in this direction.

It should also be noted that while we have demonstrated correlations between tracer binding, off-target binding has been reported for ^{18}F-AV1451 in the midbrain, lateral geniculate nucleus, choroid plexus, basal ganglia, substantia nigra, meninges, retina and melanin containing cells (Marquie et al., 2015; Lowe et al., 2016). However, this off-target binding is also likely to be present in both patients and controls and the interrogation of Z-score maps should help correct for this.

Finally, recent work has shown that ^{18}F-flutemetamol only detects later stages of amyloid deposition, universally missing Thal stages 1 and 2, and some Thal stage 3 cases (Thal et al., 2015). Consequently, some of the individuals in our 'amyloid-negative' group could have had early Alzheimer's pathology, biasing correlations between tau and microglial activation towards a positive outcome.

Implications and future directions

Our findings suggest that levels of microglial activation can correlate with tau tangle and amyloid plaque load in MCI and Alzheimer's disease. This suggests that microglial activation may play a role in propagating disease pathology in Alzheimer's disease. Certain areas of the brain are clearly more vulnerable to Alzheimer's pathology—microglial activation correlated with both amyloid deposition and tau aggregation in the posterior temporal lobe and superior frontal gyrus.

An important further area of study would focus on the cognitively healthy older control group, to detect tracer binding and pathological correlations not yet reaching clinical significance.

Further longitudinal studies in these subjects to evaluate the progression and distribution of the pathologies would allow us to better understand their underlying temporal inter-relationships.

Conclusion

This is the first PET study to examine pathological correlations between levels of microglial activation and aberrant protein aggregation in MCI and Alzheimer's disease. We found that microglial activation correlates strongly with tau aggregation in established Alzheimer disease and, to a lesser extent with amyloid deposition. In contrast, microglial activation correlates more strongly with amyloid deposition in MCI. These findings support previous *in vitro* findings and confirm the complex relationships between these pathological processes in Alzheimer's disease. Our findings suggest that a multi-targeted approach will be necessary for an effective therapeutic intervention.

Acknowledgements

Funding

Competing interests

P.E. was funded by the Medical Research Council and now by Higher Education Funding Council for England (HEFCE). He has also received grants from Alzheimer's Research, UK, Alzheimer's Drug Discovery Foundation, Alzheimer's Society, UK, Novo Nordisk, Piramal Life Sciences and GE Healthcare. He is also a consultant to Pfizer. D.J.B. has received research grants and non-financial support from the Medical Research Council, grants from Alzheimer's Research Trust, during the conduct of the study; other from GE Healthcare, personal fees from AstraZeneca, Cytox, Shire, Novartis, GSK, Navidea, UCB, and Acadia, along with grants from Michael J Fox Foundation, European Commission, the Danish council for Independent Research, and the Lundbeck Foundation outside the submitted work.

Supplementary material

Supplementary material is available at *Brain* online.

References

Bloomfield PS, Selvaraj S, Veronese M, Rizzo G, Bertoldo A, Owen DR, et al. Microglial activity in people at ultra high risk of psychosis and in schizophrenia; an [11C]PBR28 PET brain imaging study. Am J Psychiatry 2016; 173: 44–52.

Braak H, Braak E. Neuropathological staging of Alzheimer related changes in Alzheimer's disease. Acta Neuropathol 1991; 82: 239–59.

Cagnin A, Rossor M, Sampson EL, MacKinnon T, Banati R. *In vivo* detection of microglial activation in frontotemporal dementia. Ann Neurol 2004; 56: 894–7.

Casanova R, Ryali S, Baer A, Laurienti PJ, Burdette JH, Hayasaka S, et al. Biological parametric mapping: a statistical toolbox for multi-modality brain image analysis. Neuroimage 2007; 34: 137–43.

Chen W, Abud EA, Yeung ST, Lakatos A, Nassi T, Wang J, et al. Increased tauopathy drives microglia-mediated clearance of beta-amyloid. Acta Neuropathol Commun 2016; 4: 63.

Collste K, Forsberg A, Varrone A, Amini N, Aeinehband S, Yakushev I, et al. Test-rest reproducibility of [(11)C]PBR28 binding to TSPO in healthy control subjects. Eur J Nucl Med Mol Imaging 2016; 43: 173–83.

Crary JF, Trojanowski JQ, Schneider JA, Abisambra JF, Abner EL, Alafuzoff I, et al. Primary age-related tauopathy (PART): a common pathology is associated with human aging. Acta Neuropathol 2014; 128: 755–66.

Cumming P, Burgher B, Patkar O, Breakspear M, Vasdev N, Thomas P, et al. Sifting through the surfeit of neuroinflammation tracers. J Cereb Blood Flow Metab 2018; 38: 204–24.

Fan Z, Brooks DJ, Okello A, Edison P. An early and late peak in microglial activation in Alzheimer's disease trajectory. Brain 2017; 140: 792–803.

Fan Z, Calsolaro V, Atkinson RA, Femminella GD, Waldman A, Buckley C, et al. Flutriciclamide (18F-GE180) PET: first in-human PET study of novel third generatino *in vivo* marker of human translocator protein. J Nucl Med 2016; 57: 1753–9.

Fan Z, Harold D, Pasualetti G, Williams J, Brooks DJ, Edison P. Can studies of neuroinflammation in a TSPO genetic subgroup (HAB or MAB) be applied to the entire AD cohort? J Nucl Med 2015; 56: 707–13.

Gorlovoy P, Larionov S, Pham TT, Neumann H. Accumulation of tau induced in neurites by microglial proinflammatory mediators. FASEB J 2009; 23: 2502–13.

Hamelin L, Lagrade J, Dorothee G, Leroy C, Labit M, Comley RA, et al. Early and protective microglial activation in Alzheimer's disease: a prospective study using 18F-DPA-714 PET imaging. Brain 2016; 139: 1252–64.

Hammers A, Allom R, Koepp M, Free S, Myers R, Lemieux L, et al. Three-dimensional maximum probability atlas of the human brain, with particular reference to the temporal lobe. Hum Brain Mapp 2003; 19: 224–47.

Heneka MT, Carson MJ, Khoury JE, Landreth GE, Brosseron F, Feinstein DL, et al. Neuroinflammation in Alzheimer's disease. Lancet Neurol 2015; 14: 388–405.

Hines CS, Fujita M, Zoghbi SS, Kim JS, Quezado Z, Herscovitch P, et al. Propofol decreases *in vivo* binding of 11C-PBR28 to translocator protein (18 kDa) in the human brain. J Nucl Med 2013; 54: 64–9.

Ikonomovic MD, Buckley CJ, Heurling K, Sherwin P, Jones PA, Zanette M, et al. Post-mortem histopathology underlying beta-amyloid PET imaging following flutemetamol F 18 injection. Acta Neuropathol Commun 2016; 4: 130.

Ishizawa K, Dickson D. Microglial activation parallels system degeneration in progressive supranuclear palsy and corticobasal degeneration. J Neuropathol Exp Neurol 2001; 60: 647–57.

Ishizawa K, Komori T, Sasaki S, Arai N, Mizutani T, Hirose T. Microglial activation parallels system degeneration in multiple system atrophy. J Neuropath Exp Neurol 2004; 63: 43–52.

Kanegawa N, Collste K, Forsberg A, Schain M, Arakawa R, Jucaite A, et al. *In vivo* evidence of a functional association between immune cells in blood and brain in healthy human subjects. Brain Behav Immun 2016; 54: 149–57.

Kreisl WC, Fujita M, Fujimura Y, Kimura N, Jenko KJ, Kannan P, et al. Comparison of [(11)C]-(R)-PK 11195 and [(11)C]PBR28, two radioligands for translocator protein (18 kDa) in human and monkey: implications for positron emission tomographic imaging of this inflammation biomarker. Neuroimage 2010; 49: 2924–32.

Kreisl WC, Jenko KJ, Hines CS, Lyoo CH, Corona W, Morse CL, et al. A genetic polymorphism for translocator protein 18 kDa affects both *in vitro* and *in vivo* radioligand binding in human brain to this putative biomarker of neuroinflammation. J Cereb Blood Flow Metab 2013a; 33: 53–8.

Kreisl WC, Lyoo CH, Liow JS, Snow J, Page E, Jenko KJ, et al. Distinct patterns of increased translocator protein in posterior cortical atrophy and amnestic Alzheimer's disease. Neurobiol Aging 2017; 51: 132–40.

Kreisl WC, Lyoo CH, Liow JS, Wei M, Snow J, Page E, et al. (11)C-PBR28 binding to translocator protein increases with progression of Alzheimer's disease. Neurobiol Ageing 2016; 44: 53–61.

Kreisl WC, Lyoo CH, McGwier M, Snow J, Jenko KJ, Kimura N, et al. *In vivo* radioligand binding to translocator protein correlates with severity of Alzheimer's disease. Brain 2013b; 136 (Pt 7): 2228–38.

Kumar A, Muzik O, Shandal V, Chugani D, Chakraborty P, Chugani HT. Evaluation of age-related changes in translocator protein (TSPO) in human brainusing (11)C-[R]-PK11195 PET. J Neuroinflammation 2012; 9: 232.

Lee DC, Rizer J, Selenica ML, Reid P, Kraft C, Johnson A, et al. LPS-induced inflammation exacerbates phospho-tau pathology in rTg4510 mice. J Neuroinflammation 2010; 7: 56.

Lee M, McGeer E, McGeer PL. Activated human microglia stimulate neuroblastoma cells to upregulate production of beta amyloid protein and tau: implications for Alzheimer's disease pathogenesis. Neurobiol Aging 2015; 36: 42–52.

Lockhart A, Davis B, Matthews JC, Rahmoune H, Hong G, Gee A, et al. The peripheral benzodiazepine receptor ligand PK11195 binds with high affinity to the acute phase reactant α1-acid glycoprotein: implications for the use of the ligand as a CNS inflammatory marker. Nucl Med Biolgy 2003; 30: 199–206.

Logan J. Graphical analysis of PET data applied to reversible and irreversible tracers. Nucl Med Biol 2000; 27: 661–70.

Lopez-Picon FR, Snellman A, Eskola O, Helin S, Solin O, Haaparanta-Solin M, et al. Neuroinflammataion appears early and then pleatueas in a mouse model of Alzheimer's disase shown by PET imaging. J Nucl Med 2018; 59: 509–15.

Lowe VJ, Curran G, Fang P, Liesinger AM, Josephs KA, Parisi JE, et al. An autoradiographic evaluation of AV-1451 Tau PET in dementia. Acta Neuropathol Commun 2016; 4: 58.

Lyoo CH, Ikawa M, Liow JS, Zoghbi SS, Morse CL, Pike VW, et al. Cerebellum can serve as a pseudo-reference region in Alzheimer's disease to detect neuroinflammation measured with PET radioligand binding to translocator protein (TSPO). J Nucl Med 2015; 56: 701–6.

Manso Y, Holland PR, Kitamura A, Szymkowiak S, Duncombe J, Hennessy E, et al. Minocycline reduces microgliosis and improves subcortical white matter function in a model of cerebral vascular disease. Glia 2018; 66: 34–46.

Maphis N, Guixiang X, Kokiko-Cochran ON, Cardona AE, Ransohoff RM, Lamb BT, et al. Loss of tau rescues inflammation-mediated neurodegeneration. Front Neurosci 2015a; 9: 196.

Maphis N, Xu G, Kokiko-Cochran ON, Jiang S, Cardona A, Ransohoff RM, et al. Reactive microglia drive tau pathology and contribute to the spreading of pathological tau in the brain. Brain 2015b; 138 (Pt 6): 1738–55.

Marquie M, Normandin MD, Vanderburg CR, Costantino IM, Bien EA, Rycyna LG, et al. Validating novel tau positron emission tomography tracer [F-18]-AV-1451 (T807) on postmortem brain tissue. Ann Neurol 2015; 78: 787–800.

McGinnity CJ, Riano Barros DA, Rosso L, Veronese M, Rizzo G, Bertoldo A, et al. Test-retest reproducibility of quantitative binding measures of [(11)C]Ro15–4513, a PET ligand for GABAA receptors containing alpha5 subunits. Neuroimage 2017; 152: 270–82.

McKhann GM, Drachman D, Folstein M, Katzman R, Price D, Stadlan EM. Clinical diagnosis of Alzheimer's disease: report of the NINCDS-ADRDA Work Group under the auspices of the Department of Healthy and Human Services Task Force on Alzheimer's Disease. Neurology 1984; 34: 939–44.

McKhann GM, Knopman DS, Chertkow H, Hyman BT, Jack CR Jr, Kawas CH, et al. The diagnosis of dementia due to Alzheimer's disease: recommendations from the National Institute on Aging-Alzheimer's Association workgroups on diagnostic guidelines for Alzheimer's disease. Alzheimers Dement 2011; 7: 263–9.

Narendran R, Frankle WG. Comment on analyses and conclusions of 'microglial activity in people at ultra high risk of psychosis and in schizophrenia: an [11C]PBR28 PET Brain Imaging Study. Am J Psychiatry 2016; 173: 535–6.

Owen DR, Guo Q, Kalk NJ, Colasanti A, Kalogiannopoulou D, Dimber R, et al. Determination of [(11)C]PBR28 binding potential *in vivo*: a first human TSPO blocking study. J Cereb Blood Flow Metab 2014; 34: 989–94.

Owen DR, Narayan N, Wells L, Healy L, Smyth E, Rabiner EA, et al. Pro-inflammatory activation of primary microglia and macrophages increases 18 kDa translocator expression in rodents but not humans. J Cereb Blood Flow Metab 2017; 37: 2679–90.

Owen DR, Yeo AJ, Gunn RN, Song K, Wadsworth G, Lewis A, et al. An 18-kDa translocator protein (TSPO) polymorphism explains differences in binding affinity of the PET radioligand PBR28. J Cereb Blood Flow Metab 2012; 32: 1–5.

Park E, Gallezot JD, Delgadillo A, Liu S, Planeta B, Lin SF, et al. (11)C-PBR28 imaging in multiple sclerosis patients and healthy controls: test-retest reproducibility and focal visualization of active white matter areas. Eur J Nucl Med Mol Imaging 2015; 42: 1081–92.

Pascoal TA, Mathotaarachchi S, Shin M, Benedet AL, Mohades S, Wang S, et al. Synergistic interaction between amyloid and tau predicts the progression to dementia. Alzheimers Dement 2017; 13: 644–53.

Pasqualetti G, Brooks DJ, Edison P. The role of neuroinflammation in dementias. Curr Neurol Neurosci Rep 2015; 15: 17.

Paulus W, Bancher C, Jellinger K. Microglial reaction in Pick's disease. Neurosci Lett 1993; 161: 89–92.

Perl DP. Neuropathology of Alzheimer's disease. Mt Sinai J Med 2010; 77: 32–42.

Perlmutter LS, Barron E, Chui HC. Morphologic association betweem microglia and senile plaque amyloid in Alzheimer's Disease. Neurosci Lett 1990; 119: 32–6.

Petersen RC, Caracciolo B, Brayne C, Gauthier S, Jelic V, Fratiglioni L. Mild cognitive impairment: a concept in evolution. J Intern Med 2004; 275: 214–28.

Pontecorvo MJ, Devous MD Sr, Navitsky M, Lu M, Salloway S, Schaerf FW, et al. Relationships between flortaucipir PET tau binding and amyloid burden, clinical diagnosis, age and cognition. Brain 2017; 140: 748–63.

Price J, Morris J. Tangles and Plaques in nondemented aging and 'Preclinical' Alzheimer's disease. Ann Neurol 1999; 45: 358–68.

Quintanilla RA, Orellana D, Gonzalez-Billault C, Maccioni R. Interluekin-6 induces Alzheimer-type phosphorylation of tau protein by deregulating the cdk5/p35 pathway. Exp Cell Res 2004; 295: 245–57.

Rizzo G, Veronese M, Tonietto M, Zanotti-Fregonara P, Turkheimer FE, Bertoldo A. Kinetic modeling without accounting for the vascular component impaires the quantificatio of 11C-PBR28 brain PET data. J Cereb Blood Flow Metab 2014; 34: 1060–9.

Salloway S, Sperling R, Fox NC, Blennow K, Klunk W, Raskind M, et al. Two phase 3 trials of bapineuzumab in mild-to-moderate Alzheimer's disease. N Engl J Med 2014; 370: 322–33.

Schneider JA, Arvanitakis Z, Leurgans SE, Bennett DA. The neuropathology of probable Alzheimer's disease and mild cognitive impairment. Ann Neurol 2009; 66: 200–8.

Serrano-Pozo A, Betensky RA, Frosch MP, Hyman BT. Plaque-associated local toxicity increases over the clinical course of Alzheimer disease. Am J Pathol 2016; 186: 375–84.

Serrano-Pozo A, Frosch MP, Masliah E, Hyman BT. Neuropathological alterations in Alzheimer disease. Cold Spring Harb Perspect Med 2011a; 1: a006189.

Serrano-Pozo A, Mielke ML, Gomez-Isla T, Betensky RA, Growdon JH, Frosch MP, et al. Reactive glia not only associates with plaques but also parallels tangles in Alzheimer's disease. Am J Pathol 2011b; 179: 1373–84.

Serrano-Pozo A, Qian J, Monsell SE, Blacker D, Gomez-Isla T, Betensky RA, et al. Mild to moderate Alzheimer dementia with insufficient neuropathological changes. Ann Neurol 2014; 75: 597–601.

Sheffield LG, Marquis J, Berman NE. Regional distribution of cortical microglia parallels that of neurofibrillary tangles in Alzheimer's disease. Neurosci Lett 2000; 285: 165–8.

Shidahara M, Tsoumpas C, Hammers A, Boussion N, Visvikis D, Suhara T, et al. Functional and structural synergy for resolution recovery and partial volume correction in brain PET. Neuroimage 2009; 44: 340–8.

Stalder M, Phinney A, Probst A, Sommer B, Staufenbiel M, Jucker M. Association of microglia with amyloid plaques in brain of APP23 transgenic mice. Am J Pathol 1999; 154: 1673–84.

Surendranathan A, Rowe JB, O'Brien JT. Neuroinflammation in Lewy body dementia. Parkinsonism Relat Disord 2015; 21: 1398–406.

Suridjan I, Rusjan PM, Voineskos AN, Selvanathan T, Setiawan E, Strafella AP, et al. Neuroinflammation in healthy aging: a PET study using a novel Translocator Protein 18 kDa (TSPO) radioligand [(18)F]-FEPPA. Neuroimage 2014; 84: 868–75.

Thal DR, Beach TG, Zanette M, Heurling K, Chakrabarty A, Ismail A, et al. [(18)F]flutemetamol amyloid positron emission tomography in preclinical and symptomatic Alzheimer's disease: specific detection of advanced phases of amyloid-B pathology. Alzheimers Dement 2015; 11: 975–85.

Turkheimer FE, Rizzo G, Bloomfield PS, Howes O, Zanotti-Fregonara P, Bertoldo A, et al. The methodology of TSPO imaging with positron emission tomography. Biochem Soc Trans 2015; 43: 586–92.

Vasconcelos B, Stancu IC, Buist A, Bird M, Wang P, Vanoosthuyse A, et al. Heterotypic seeding of Tau fibrillization by pre-aggregated Abeta provides potent seeds for prion-like seeding and propagation of Tau-pathology in vivo. Acta Neuropathol 2016; 131: 549–69.

Vidale S, Consoli A, Arnaboldi M, Consoli D. Postischemic inflammation in acute stroke. J Clin Neurol 2017; 13: 1–9.

Villemagne V, Burnham S, Bourgeat P, Brown B, Ellis K, Salvado O, et al. Amyloid B deposition, neurodegeneration, and cognitive decline in sporadic Alzheimer's disease: a prospective cohort study. Lancet 2013; 12: 357–67.

Walker MD, Dinelle K, Kornelsen R, Lee NV, Miao Q, Adam M, et al. [C]PBR28 PET imaging is sensitive to neuroinflammation in the aged rat. J Cereb Blood Flow Metab 2015; 35: 1331–8.

Xia CF, Arteaga J, Chen G, Gangadharmath U, Gomez LF, Kasi D, et al. [(18)F]T807, a novel tau positron emission tomography imaging agent for Alzheimer's disease. Alzheimers Dementia 2013; 9: 666–76.

Yoder KK, Nho K, Risacher SL, Kim S, Shen L, Saykin AJ. Influence of TSPO genotype on 11C-PBR28 standardized uptake values. J Nucl Med 2013; 54: 1320–2.

Yoshiyama Y, Higuchi M, Zhang B, Huang SM, Iwata N, Saido TC, et al. Synapse loss and microglial activation precede tangles in a P301S tauopathy mouse model. Neuron 2007; 53: 337–51.

Zhao SC, Ma LS, Chu ZH, Xu H, Wu WQ, Liu F. Regulation of microglial activation in stroke. Acta Pharmacol Sin 2017; 38: 445–58.

Zilka N, Stozicka Z, Kovac A, Pilipcinec E, Bugos O, Novak M. Human misfolded truncated tau protein promotes activation of microglia and leukocyte infiltration in the transgenic rat model of tauopathy. J Neuroimmunol 2009; 209: 16–25.